Au_N clusters ($N = 1$–6) supported on MgO(100) surfaces: Effect of exact exchange and dispersion interactions on adhesion energies

Lauro Oliver Paz-Borbón,[1,*] Giovanni Barcaro,[2] Alessandro Fortunelli,[2] and Sergey V. Levchenko[1]

[1]*Fritz Haber Institute of Max Planck Society, Faradayweg 4-6, DE-14195, Berlin-Dahlem, Germany*

[2]*CNR-IPCF, Istituto per i Processi Chimico-Fisici del Consiglio Nazionale delle Ricerche, via G. Moruzzi 1, IT-56124, Pisa, Italy*

(Received 8 July 2011; revised manuscript received 31 January 2012; published 4 April 2012)

The energetics of an Au adatom and Au_N clusters ($N = 2$–6) supported on pristine and reduced MgO(100) surfaces is analyzed using an all-electron full-potential density functional theory approach. A hierarchy of exchange-correlation functional approximations is employed, ranging from the generalized gradient approximation [Perdew-Burke-Ernzerhof (PBE), revised PBE (RPBE)] to hybrid functionals [PBE0, Heyd-Scuseria-Ernzerhof (HSE06)] to exact exchange plus correlation in the random phase approximation (EX-cRPA/cRPA+). The analysis of different terms in the electronic Hamiltonian, contributing to calculated adhesion energies (E_{adh}) for the Au adatom, shows that reducing the self-interaction error leads to smaller E_{adh} values. On the contrary, the energy barriers for diffusion of an Au adatom at the pristine surface significantly increase. For Au_N clusters ($N > 1$), dispersion effects, not accounted for by the generalized gradient approximation or hybrid functionals, start to make an increasingly important contribution to the adhesion energy.

DOI: 10.1103/PhysRevB.85.155409 PACS number(s): 68.47.Jn, 73.22.−f, 71.15.Mb

I. INTRODUCTION

Gold catalysts have been the subject of a vast number of experimental and theoretical studies since the breakthrough discovery by Haruta *et al*. of the catalytic properties of Au nanoparticles.[1,2] The catalytic activity of Au nanoparticles was demonstrated for several chemical reactions of practical interest, such as hydrogenation of olefins,[3] propene epoxidation,[4,5] reduction of nitrogen oxides,[6] water-gas shift reaction,[7] as well as CO oxidation.[8–10]

In order to be used as heterogeneous catalysts, metal nanoparticles must be immobilized on a solid surface. The stronger the interaction with the support, the more stable are the nanoparticles with respect to sintering. However, the strong interaction can substantially influence the chemical properties of the supported nanoparticles. Therefore, it is very important to understand the electronic and geometric structure factors governing the nanoparticle-support interaction and the chemical properties of the resulting material.

Using oxide materials as a support opens a unique and immense field of possibilities for tuning the physical and chemical properties of the nanoparticles.[11–13] However, stoichiometry, as well as geometric and electronic structure of oxide surfaces (in particular, concentration of point defects and their charge state), can change depending on experimental conditions, and it is often quite difficult to characterize such changes experimentally. Therefore, in order to build up fundamental understanding of the metal-support interaction, it is desirable to use an oxide supporting material with well-characterized surfaces that are stable in a wide range of temperatures and chemical environments.

From this point of view, the (100) surface of MgO was demonstrated to be a suitable model system.[14–17] Pristine MgO(100) surfaces can be prepared by various techniques with low concentration of both point and extended defects (steps). Under ultrahigh vacuum conditions, point defects, in particular oxygen vacancies (neutral and positively charged), can be created using electron bombardment and doping with alkali metals.[18–21]

Surface oxygen vacancies (F_s centers) interact strongly with metal atoms, serving as nucleation centers for nanoparticle growth, or acting as an anchoring point which prevents the diffusion of soft-landed particles.[22–29] The effect of an F_s center on the supported metal nanoparticle is twofold: (i) the vacancy can donate or accept electrons from the particle (depending on the initial charge of the vacancy),[30] and (ii) it can cause a rearrangement of the particle's atomic structure with respect to its corresponding gas-phase structure,[31] in particular due to the charge redistribution between the metal nanoparticles and the vacancy.[32–37]

Accurate knowledge of the potential energy surface underlying interaction of metal clusters with the support is very important for understanding and interpretation of experimental results on the supported nanoparticles. Surprisingly, experimental determination of adhesion energies of Au clusters on MgO(100) has not been reported. However, the interaction of an Au adatom and small Au_N clusters with pristine and F_s-defected MgO(100) surfaces has been extensively studied theoretically in the last decade using density functional theory (DFT) with local density (LDA) and generalized gradient (GGA) approximations to the exchange-correlation (XC) functional.[11,12,38–53] These studies have agreed on the oxygen surface site as the preferred adsorption site for the Au adatom on the pristine MgO(100) surface, as has been recently confirmed by electron paramagnetic resonance (EPR) spectroscopy.[54,55] However, the LDA and GGA XC functionals are known to suffer from the self-interaction error (SIE), especially in cases where accurate description of electron localization plays an important role (for example, in ionic materials). Underestimation of the electron localization on the MgO surface oxygen anion can lead to overestimation of the strength of interaction between the surface and the adsorbed metal clusters and an underestimation of diffusion barriers.[56,57] Moreover, the standard XC functionals do not describe correctly the van der Waals interaction. Both O^{2-} anion in MgO lattice (or a neutral oxygen vacancy) and Au clusters can be anticipated to have large polarizabilities, and,

therefore, the van der Waals interaction can have a profound effect on the cluster adhesion energies.

Thus, an accurate theoretical modeling of the interaction of Au nanoparticles with MgO(100) surfaces is still lacking. Such modeling is challenging due to the extended nature of the oxide surface and the large configurational space to be explored, which put practical restrictions on the level of theory that can be used. In this respect, a combination of exact exchange with correlation in the random phase approximation (EX-cRPA) as formulated within the adiabatic connection fluctuation-dissipation (ACFD) theorem, looks very promising. EX-cRPA has been recently demonstrated to be one of the most accurate post-DFT methods providing excellent results for lattice constants, bulk moduli, as well as adsorption and surface energies.[58,59] It is free of SIE since it incorporates the exact exchange (EX), describes correctly screening of the Coulomb potential, and seamlessly includes nonlocal van der Waals (vdW) forces as part of its formalism.[60–66] Nowadays, due to the increase in computational power and development of robust computational algorithms efficiently scalable to a large number of processors, EX-cRPA calculations have become feasible for application to realistic systems such as small molecules,[62,63] atoms and clusters,[64] layered systems,[65] as well as molecules adsorbed on metal surfaces.[60,66]

The aim of this work is to analyze in detail the effects of exchange and correlation on the potential energy surface (PES) for adsorption of a gold atom and small Au_N clusters ($N = 2$–6) on pristine and O-deficient MgO(100) surfaces. We apply a hierarchy of XC functionals, ranging from the generalized gradient approximation [Perdew-Burke-Ernzerhof (PBE), revised PBE (RPBE)] through hybrid functionals [PBE0, Heyd-Scuseria-Ernzerhof (HSE06)] to exact exchange (EX) plus correlation in the random phase approximation (EX-cRPA) and its short-range correction (EX-cRPA+).[67] Furthermore, we have also applied a dispersion-corrected functional (PBE–vdW) based on the recently developed Tkatchenko-Scheffler scheme[68] to analyze the contribution of vdW interaction to the calculated adhesion energies (E_{adh}).

II. COMPUTATIONAL DETAILS

The FHI-aims electronic-structure package[69] is used to calculate the adhesion energies (E_{adh}) of an Au adatom and Au_N ($N = 2$–6) clusters supported on both pristine and neutral F_s-defected MgO(100) surfaces. E_{adh} are calculated as the total energy differences between the interacting system and its corresponding frozen fragments:

$$E_{adh} = -[E(Au_N/MgO_{site}) - E(MgO_{site}) - E(Au_N)]. \quad (1)$$

In FHI-aims, the Kohn-Sham (KS) equations are solved using numerical atom-centered orbitals (NAOs) as basis functions. Relativistic effects are included within the scaled zeroth-order relativistic approximation (ZORA).[70] Calculations have been performed using a spin-polarized formalism.

A. Approximations to the XC functional

The selection of the above-mentioned XC functionals is motivated by their gradual increase in accuracy (at the expense of CPU time), according to Perdew's "DFT Jacob's ladder" for XC functionals.[71] In this sense, the GGA corresponds to the second rung of Jacob's ladder (LDA being the first). The PBE functional was selected due to the fact that it is one of the most successful nonempirical GGA functionals,[72] while its revised version (RPBE) was also tested as it has been claimed to work better than PBE for atomization energies of molecules, lattice constants, and surface energies of solids, but worse than PBE for molecular bond lengths.[73] The use of hybrid functionals represents climbing two steps higher (to the fourth rung) in the XC hierarchy, as they incorporate a fraction of Hartree-Fock exchange, which partially reduces SIE. In this work, we employ the nonempirical hybrid functional PBE0.[74,75] We also test the performance of the HSE06 functional, in which the Coulomb potential is partitioned into a short- and a long-range part, with the exact exchange included only for the short-range part.[76] This separation reduces the computational cost of exact exchange calculations, especially for periodic systems, at the expense of introducing a new (screening) parameter.

Finally, the fifth DFT rung is reached through the adiabatic connection, which leads to generalizations of the random-phase approximation (EX-cRPA).[60–66] Performing EX-cRPA calculations is currently an extremely computationally demanding task, and is commonly done as non-self-consistent post correction to a preceding standard DFT calculation.[60] In our work, the EX-cRPA calculations are based on PBE orbitals. In FHI-aims, EX-cRPA total energies are computed as

$$E_{total}^{RPA}[\{\psi_N\}] = E_{total}^{DFT} - E_{xc}^{DFT} + E_x[\{\psi_N\}] + E_c^{RPA}[\{\psi_N\}], \quad (2)$$

where the exchange-correlation energy (E_{xc}^{DFT}) of the chosen DFT functional is replaced by the exchange-correlation energy in EX-cRPA, i.e., $E_x[\{\psi_N\}]$ corresponds to the Hartree-Fock expression for the exchange energy, evaluated using DFT (PBE) orbitals, while the EX-cRPA correlation energy $E_c^{RPA}[\{\psi_N\}]$,

$$E_c^{RPA} = \frac{1}{2\pi}\int_0^\infty du\, \mathrm{Tr}\{\ln[1 - \chi_0(iu)v] + \chi_0(iu)v\}, \quad (3)$$

is calculated within the ACFD theorem.[60] Here [Eq. (3)], $\mathrm{Tr} = \int d\mathbf{r}\int d\mathbf{r}'$, $v = 1/|\mathbf{r}\text{-}\mathbf{r}'|$ corresponds to the bare Coulomb potential, and χ_0 is the dynamic-response function of the noninteracting KS system. The calculation of χ_0 involves both occupied and unoccupied KS spin orbitals $\psi_{n\sigma}$, their energies $\epsilon_{n\sigma}$, and their occupations $f_{n\sigma}$:

$$\chi_0(\mathbf{r},\mathbf{r}',iu) = \sum_\sigma \sum_{mn} \frac{(f_{m\sigma} - f_{n\sigma})}{iu + \epsilon_{n\sigma} - \epsilon_{m\sigma}} \times \psi_{m\sigma}^*(\mathbf{r})\psi_{n\sigma}(\mathbf{r})\psi_{n\sigma}^*(\mathbf{r}')\psi_{m\sigma}^*(\mathbf{r}'). \quad (4)$$

An important consideration regarding EX-cRPA is that, although RPA is exact for long-range electron-electron correlation, it poorly approximates short-range correlation.[67] In FHI-aims, EX-cRPA is short-range corrected according to the Kurth and Perdew method,[67] resulting in EX-cRPA+. This correction (small but not negligible) is calculated in FHI-aims and included in our results.

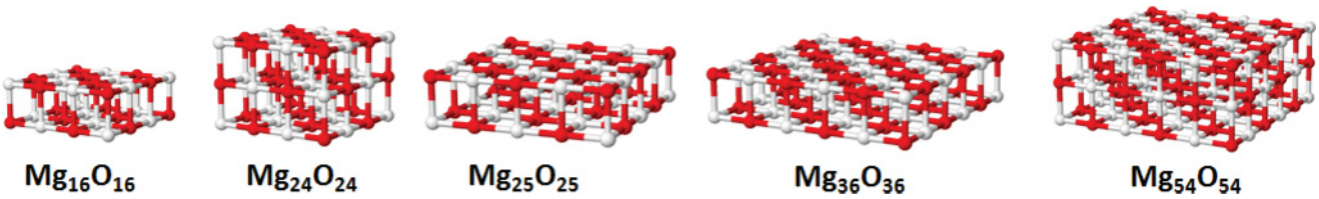

FIG. 1. (Color online) MgO(100) cluster surface models. The two-layer $Mg_{16}O_{16}$ cluster is used to map the Au adatom PES, while the two-layer $Mg_{25}O_{25}$ clusters are used to calculate the corresponding E_{adh} values of Au_N clusters at both pristine and F_s-defected surfaces.

B. MgO(100) surface models

We use cluster models of the MgO(100) surface embedded in an array of point charges (PC). The quality of the embedding is tested at the PBE level by comparing the results of cluster calculations to periodic models. In the periodic calculations, the MgO(100) surface is modeled by a three-layer $Mg_{54}O_{54}$ slab (i.e., 3 × 3 having 18 Mg and 18 O atoms per layer), which has been checked to produce E_{adh} values converged (errors below 10 meV) with respect to the number of layers and the lateral distance between periodic images. The simulation box is chosen with a height of 21.04 Å, assuring no interaction between images in the direction normal to the surface (closest distance between images is ∼10 Å). In order to simulate a surface of semi-infinite crystal, the bottom layer of the MgO slab is held frozen at the rock-salt bulk structure with the experimental lattice constant of 4.208 Å, as used in previous theoretical work.[11] The surface and middle layers are fully relaxed in the periodic calculations, for both pristine and F_s-defected MgO(100) surfaces.

Periodic (PBE) relaxations were performed using FHI-aims *light* settings, *tier*-1 basis set (roughly of double-zeta plus polarization functions, DZPV, quality for Mg and Au, but slightly reduced for oxygen, if compared to Gaussian basis sets)[77] and a (2 × 2 × 1) k-point mesh for the Brillouin zone sampling, while single-point calculations were then performed on the relaxed geometries using *tight* numerical settings (but with basis set increased to *tier* 2 for Au and Mg) and a (4 × 4 × 1) k-point mesh.

The convergence with basis-set size was tested by performing calculations with a *tier*-3 basis set, and the errors were below 10 meV (see Refs. 69 and 77 for the exact meaning of these settings). Since EX-cRPA/cRPA+ methods are not yet implemented in FHI-aims for periodic systems, MgO(100) cluster models embedded in an array of 20 × 20 × 5 point charges (±2.0 a.u.) are used.[78] In all cluster models, the positions of Mg and O atoms, including PCs, correspond to the experimental lattice constant. In all cluster calculations, surface relaxation was not carried out. For PBE, the difference between gold atom adhesion energies calculated with the relaxed periodic surface model and the unrelaxed cluster models (but with optimized Au-surface distance) was of the order of ∼0.1 eV. Each pristine MgO(100) cluster model has equal number of O and Mg atoms. Single-point energy calculations were performed using the *tight* settings and *tier*-2 basis set for all species.

Dependence of E_{adh} values on cluster size for an Au adatom, adsorbed at both oxygen and F_s center sites, is studied using different cluster models: from a two-layer $Mg_{16}O_{16}$, three-layer $Mg_{24}O_{24}$, two-layer $Mg_{25}O_{25}$, two-layer $Mg_{36}O_{36}$, up to the three-layer $Mg_{54}O_{54}$ (see Fig. 1 and Tables I and II). For the Au atom on the pristine surface, the EX-cRPA/cRPA+ E_{adh} values are nearly converged for the two-layer $Mg_{25}O_{25}$ cluster model. The same model is used for the Au_N (N = 2–6) clusters. In this model, none of the Au atoms touch the border of the embedded MgO cluster.

For the F_s center calculations, the same cluster models as described above are used. Here, the absolute convergence is worse than in the case of the pristine surface. In particular, the dependence on the number of layers is more pronounced, but also the convergence with lateral size is slower. Nevertheless, the dependence on the XC treatment is qualitatively the same for all cluster sizes, which is sufficient for the purposes of this paper.

We validated the use of the periodic PBE Au adatom/oxide surface distances $Z_{(Au\text{-}surface)}$, obtained for each adsorption site (see Table III), by performing a constrained optimization of $Z_{(Au\text{-}surface)}$ for the smallest cluster model. In these calculations, $Z_{(Au\text{-}surface)}$ was constrained to different values obtained by varying the optimal distance by ±6% with ±2% intervals with respect to the periodic PBE value, for all XC functionals. In the case of EX-cRPA/cRPA+ and the hybrid functionals, the corresponding equilibrium positions, for all adsorption sites, lie within less than 4% difference with respect to the periodic PBE distance (the corresponding differences in E_{adh} are of the order of ∼10 meV). For the RPBE functional, we observed slightly larger differences (∼50 meV). However, RPBE is known to give less accurate geometries compared to PBE.[71] This test gave us confidence to use the $Z_{(Au\text{-}surface)}$ distances (and Au_N geometries), optimized from periodic PBE calculations, in our cluster models. All the calculated E_{adh} values were corrected for the basis-set superposition error (BSSE) using the counterpoise method of Boys and Bernardi.[79]

TABLE I. E_{adh} convergence, as a function of MgO(100) cluster size, for an Au adatom adsorbed at the oxygen site. Dashes indicate hybrid functional and EX-cRPA/cRPA+ calculations for which basis-set convergence could not be reached due to CPU/memory limitations.

E_{adh} (eV)	$Mg_{16}O_{16}$	$Mg_{24}O_{24}$	$Mg_{25}O_{25}$	$Mg_{36}O_{36}$	$Mg_{54}O_{54}$
PBE	0.93	0.92	0.85	0.87	0.87
RPBE	0.61	0.60	0.53	0.55	0.55
HSE06	0.75	0.75	0.67	0.70	–
PBE0	0.73	0.73	0.65	0.67	–
EX-cRPA	0.69	0.70	0.65	0.68	–
EX-cRPA+	0.66	0.67	0.62	0.66	–

TABLE II. E_{adh} convergence, as a function of MgO(100) cluster size, for the Au adatom adsorbed at the F_s center site. Dashes indicate hybrid functional and EX-cRPA/cRPA+ calculations for which basis-set convergence could not be reached due to CPU/memory limitations.

E_{adh} (eV)	$Mg_{16}O_{15}$	$Mg_{24}O_{23}$	$Mg_{25}O_{24}$	$Mg_{36}O_{35}$	$Mg_{54}O_{53}$
PBE	2.96	3.07	2.97	2.98	3.16
RPBE	2.59	2.70	2.60	2.61	2.79
HSE06	2.70	2.79	2.71	2.74	–
PBE0	2.66	2.71	2.67	2.71	–
EX-cRPA	2.84	2.91	2.84	2.84	–
EX-cRPA+	2.78	2.86	2.78	2.78	–

III. RESULTS AND DISCUSSION

A. Au adatom at pristine and F_s-defected MgO(100)

Previous theoretical work on the adsorption of an Au adatom on the pristine MgO(100) surface has highlighted the preference of Au to bind at the five-coordinated oxygen site, with calculated E_{adh} values ranging from approximately 0.5 to 1 eV, using semilocal (mostly RPBE, PBE, and PW91) XC functionals.[11,44,49,51,80] Recent EPR spectroscopy studies confirm this preference.[54,81] It has been rationalized by the atom polarization in the Madelung field, which favors anionic over cationic sites for metallic adsorbates on highly ionic oxide materials.[48,82] Moreover, a hybridization of the Au 6*s* and 5*d* orbitals with the 2*p* states of the surface oxygen promotes the formation of weak covalent bonds, which further strengthens this interaction.[11,49,82] In our calculations, we observe the preference of Au to bind to the surface anion site on the pristine MgO(100) surface for all five XC functionals (see Table III), with the calculated PBE and RPBE E_{adh} values and the Au adatom-surface distance being in agreement with previous theoretical work.[11,44,49,51,80]

Climbing up the XC ladder, we notice that the inclusion of a fraction of Hartree-Fock exchange (25%) in the PBE0 and HSE06 hybrid functionals has a considerable effect on the calculated E_{adh} values, as they decrease from 0.93 eV at PBE level to 0.73 and 0.75 eV, respectively. Hybrid functionals, such as B3LYP,[83] have been previously used to study Au atom adsorbed at different MgO(100) sites. Using a small two-layer Mg_9O_9 cluster model (embedded in PCs), Di Valentin *et al.* reported an E_{adh} value of 0.77 eV for the Au adatom adsorbed at the oxygen site.[84] Similarly, Ferrullo *et al.* have recently reported a B3LYP E_{adh} value of 0.73 eV (BSSE corrected) using a slightly larger $Mg_{13}O_{13}$ model.[85]

TABLE III. Calculated E_{adh} values for an Au adatom adsorbed on the two-layer $Mg_{16}O_{16}$ cluster at different surface sites for the five XC functionals considered in this study. Optimal PBE $Z_{(Au\text{-}surface)}$ distances are obtained by constraining the *x* and *y* coordinates of the Au adatom and relaxing the *z* distance for each adsorption site (distances are given in Å).

E_{adh} (eV)	PBE	HSE06	PBE0	EX-cRPA/cRPA+	RPBE	$Z_{(Au\text{-}surface)}$
Oxygen	0.93	0.75	0.73	0.69/0.66	0.61	2.29
Magnesium	0.53	0.27	0.24	0.13/0.11	0.33	2.75
Bridge	0.68	0.45	0.42	0.37/0.34	0.37	2.37
Hollow	0.69	0.45	0.42	0.38/0.35	0.40	2.42
F_s center	2.96	2.70	2.66	2.84/2.78	2.59	1.83

At the fifth DFT rung (EX-cRPA/cRPA+), we obtained slightly smaller E_{adh} values compared to those calculated using semilocal (PBE) and the hybrid functionals. The calculated EX-cRPA/cRPA+ E_{adh} values are 0.69 and 0.66 eV, respectively. By comparing the results shown in Table III, one can observe that the calculated E_{adh} values tend to be smaller as one improves the treatment of exchange and correlation (with the exception of RPBE, for which the form of the exchange potential is modified with respect to PBE to give improved atom total energies and molecular atomization energies, at the same time ensuring fulfillment of the integrated Lieb-Oxford bound[73]). Thus, the calculated E_{adh} values follow the trend: PBE (0.93 eV) > PBE0, HSE06 (0.73 and 0.75 eV) > EX-cRPA/cRPA+ (0.69 and 0.66 eV). These results clearly suggest that there is a weakness inherent to standard XC functionals that prevents them from correctly describing the metal atom-surface interaction.

For the F_s center, our calculated E_{adh} values are about 2 eV larger compared to the pristine surface, for all functionals (see Tables II and III). The enhancement of E_{adh} values for neutral F_s center is attributed to the presence of relatively weakly bound electrons associated with the defect, which can readily interact with the metal atom.[11,49] This explains why F_s centers play a critical role in the nucleation and growth of metal nanoparticles as seen from STM experiments[16,86] and suggests how the F_s centers could modify chemical properties of the supported particles.[11,30,44,51] Our E_{adh} values compare well with previous work [3.04–3.17 eV for PW91,[11,49] ∼2.5 eV for RPBE,[51] and 2.89–2.93 for hybrid B3LYP (Refs. 84 and 85) XC functionals]. It is interesting to note that, contrary to the case of Au atom adsorption on the pristine surface, EX-cRPA/cRPA+ gives *larger* adhesion energies compared to hybrid functionals, while RPBE still gives lower E_{adh} values (Table III). This indicates that not only exchange, but also correlation effects, in particular the van der Waals interaction, start to play an important role in the interaction of a Au atom with an F_s center since among the considered approaches, only RPA incorporates ionic, covalent, and van der Waals interactions seamlessly in one scheme.[59]

In order to understand the dependence of the calculated E_{adh} values on the XC functional for the Au adatom adsorbed at the oxygen site, we decompose E_{adh} into kinetic energy (E_k^F), electrostatic energy ($E_{electro}^F$) (including Hartree energy and the electron-nuclear attraction energy), and the exchange (E_x^F) and correlation (E_c^F) energy contributions. Figure 2 shows these contributions as a function of Au-O^{2-} distance within a ±6% range of the PBE equilibrium distance. Each energy contribution is calculated in analogy with Eq. (1), but without the minus sign in front of the square brackets, i.e., negative (positive) values correspond to attractive (repulsive) interactions. The absolute value of the total sum of these contributions leads to the calculated E_{adh} values ($E_{adh} = E_{electro}^F + E_k^F + E_x^F + E_c^F$). This approach has been used very recently to study the role of nonlocal correlations for the cohesive properties of coinage metals.[87]

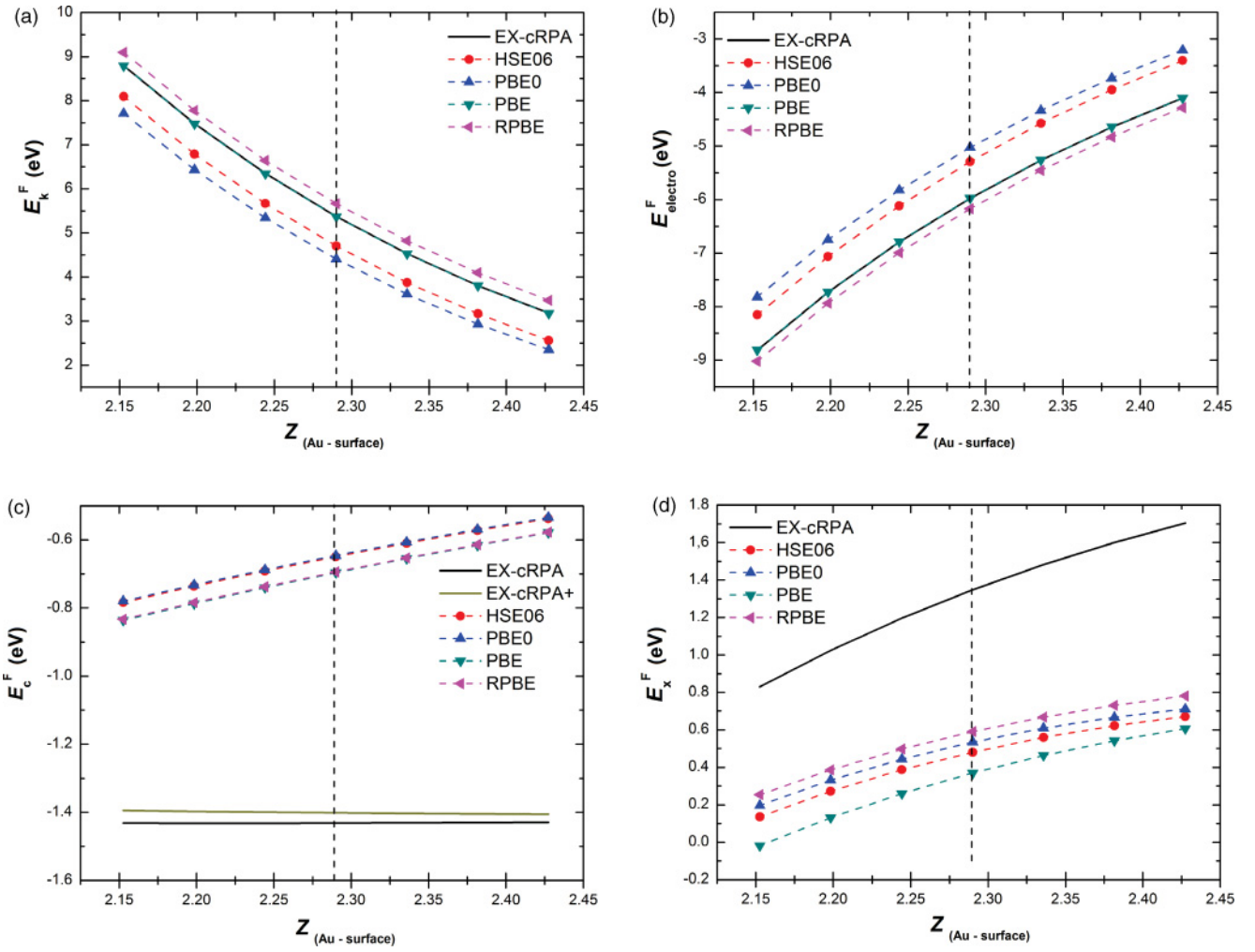

FIG. 2. (Color online) Decomposition of E_{adh} values (for the Au adatom adsorbed on the oxygen site of the $Mg_{16}O_{16}$ cluster) into (a) E_k^F, (b) $E_{electro}^F$, (c) E_c^F, and (d) E_x^F energy contributions (defined in the main text) for the five XC functionals, as a function of the distance to the surface oxygen anion $Z_{(Au\text{-}surface)}$ expressed in Å.

We would like to stress that shown on Fig. 2 are the *differences* in values of each contribution between the combined Au-surface system, on one hand, and the separated surface and Au atom, on the other hand. By comparing the plots from Figs. 2(a) and 2(b), one can observe that at the equilibrium position (2.29 Å), the electrostatic energy difference ($E_{electro}^F$) dominates over the kinetic energy difference (E_k^F) for all the five XC functionals. In fact, the change in electrostatic energy accounts for 0.506 eV (RPBE), 0.591 eV (HSE06), 0.605eV (PBE and EX-cRPA/cRPA+), and 0.619 eV (PBE0) of the total E_{adh} values for each XC functional, becoming the largest contribution to the overall adsorption energy (see Fig. 3), which only slightly depends on the XC treatment, except RPBE, which stands out of the other functionals. Thus, the role of the exchange (E_x^F) and correlation (E_c^F) contributions becomes decisive to determine the E_{adh} values. Note that the electrostatic energy is always lower for the combined system, with the difference decreasing at smaller Au-surface distances, indicating that around the equilibrium distance, the system is in the regime when the Au-surface electron-nuclear attraction dominates the electron-electron repulsion, consistent with the picture of the dominating role of polarization and covalent bonding.

In order to determine the role of exact exchange, let us focus on the differences between PBE and PBE0 functionals. It is easy to check that the reduction in the adsorption energy upon inclusion of 25% of exact exchange in PBE0 is largely due to the difference in exchange energy: the difference in exchange energies between the combined and separated systems is higher for PBE0 than for PBE. Physically, this implies that the exchange of electrons between the Au atom and the surface costs more energy at the PBE0 level, consistent with the notion of reduced self-interaction error, which leads to overestimation of electron delocalization and transfer. Note that in case of RPBE, the exchange difference also makes a dominating contribution to the total adsorption energy (larger than the electrostatic plus kinetic energy terms), although to a lesser extent than in the case of PBE0.

The differences in EX-cRPA/cRPA+ exchange and correlation energy contributions considered separately are quite large [see Figs. 2(c) and 2(d)]. This is due to the fact that the EX-cRPA/cRPA+ energies are calculated

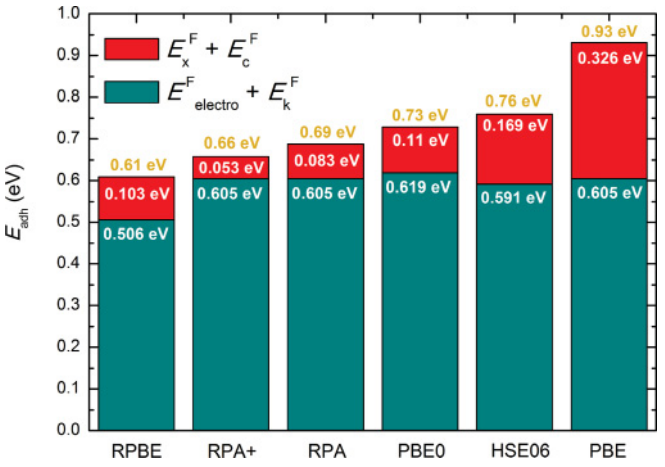

FIG. 3. (Color online) Energy contributions $E^F_{electro}+E^F_k$ (blue) and $E^F_x+E^F_c$ (red) to calculated E_{adh} values for the Au adatom adsorbed on the oxygen site of the $Mg_{16}O_{16}$ cluster for each of the five XC functionals considered in this study.

non-self-consistently on PBE orbitals. Nevertheless, one can easily see that the exchange energy difference is again dominating. By analyzing Figs. 2(c) and 2(d), one can also observe that the sum of the exchange and correlation contributions is relatively small for EX-cRPA and EX-cRPA+, accounting for 0.083 and 0.053 eV, respectively. These differences become slightly larger for the hybrid functionals, where we are only including 25% of EX, with differences of 0.11 eV for PBE0 and 0.17 eV for HSE06 (see Fig. 3). Thus, in conclusion, we find that reducing the self-interaction error plays a crucial role in calculating accurate adhesion energies of an Au adatom on the MgO surface.

TABLE IV. Energy barriers $E_{barrier}$ for Au adatom (adsorbed on the $Mg_{16}O_{16}$ cluster) diffusing along the O-hollow-O path, calculated using the five different approximations to the XC functional.

$E_{barrier}$ (eV)	RPBE	PBE	HSE06	PBE0	EX-cRPA/cRPA+
O-hollow-O	0.21	0.24	0.30	0.31	0.31/0.31

B. Au adatom diffusion energy barriers

From the E_{adh} values obtained by performing a constrained optimization of the Au adatom distance to the oxide surface at several symmetry-inequivalent adsorption sites, using a polynomial fit of the obtained values, we find that the minimum energy path lies along the straight line connecting two nearest-neighbor anion sites, with the transition state at the hollow site. The highest $E_{barrier}$ values are found for EX-cRPA/cRPA+ and the hybrid PBE0 functional (0.31 eV), closely followed by HSE06 (0.30 eV). Lower $E_{barrier}$ values are instead found for the semilocal PBE and RPBE functionals, 0.24 and 0.21 eV, respectively (see Table IV). These values are obtained for the $Mg_{16}O_{16}$ cluster model. The use of this small model for PES analysis is justified by comparison with PBE and RPBE $E_{barrier}$ values (0.26 and 0.22 eV, respectively) calculated using the relaxed periodic model with the unit cell identical to the largest cluster $Mg_{54}O_{54}$. Previous theoretical studies have reported $E_{barrier}$ values of the order of 0.20–0.24 eV, using semilocal PBE and PW91 functionals.[12,49,50] Using the Arrhenius formula $\Gamma = \Gamma_0 \exp^{-(E_{barrier}/k_B T)}$ from the transition-state theory (with a prefactor $\Gamma_0 = 10^{-13}$ s^{-1}),[50,88] one can estimate the lifetime of a Au atom at the adsorption site (so-called residence time) for the considered XC functionals. An $E_{barrier}$ value of 0.30 eV, implying residence times of less than one second, translates into diffusion temperatures of the order of 120–130 K, while $E_{barrier}$ values calculated using PBE

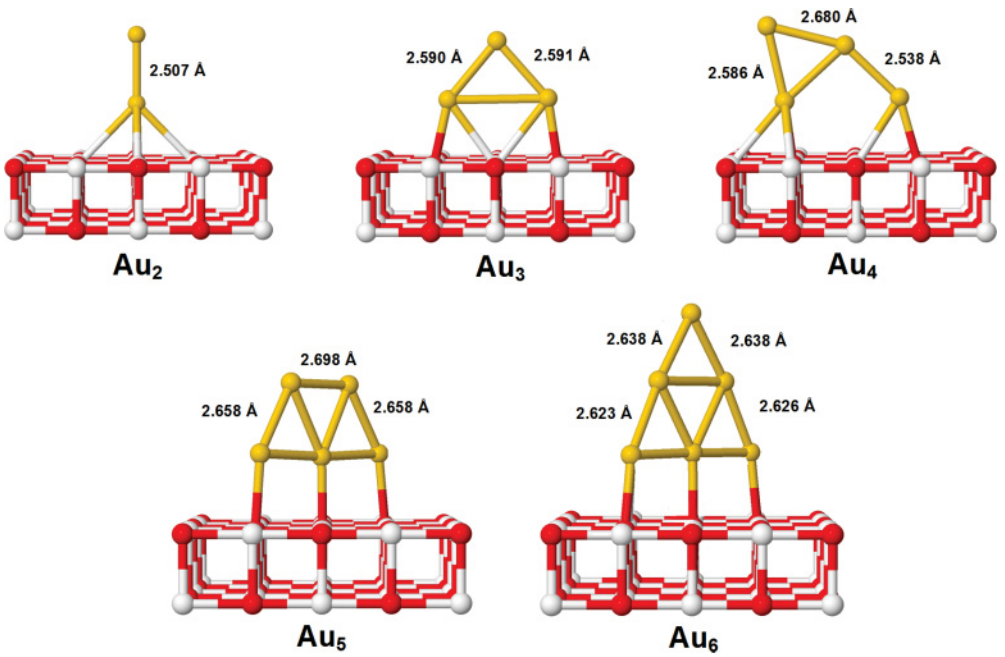

FIG. 4. (Color online) Lowest-energy (PBE) structures of Au_N (N = 2–6) clusters supported on a pristine $Mg_{25}O_{25}$ cluster surface. Bond distances are expressed in Å.

(0.24 eV) and RPBE (0.21 eV) imply Au adatom mobility temperatures of less than 100 K. In a recent experimental study, Yulikov *et al.*[55] determined the onset temperature for Au adatom diffusion on a single-crystalline film of MgO grown on Mo(100). They found a decrease of the EPR signal, attributed to isolated Au atoms adsorbed on the surface, at temperatures above 125 K, which was interpreted as a result of diffusion of Au adatom leading to Au cluster formation. Thus, our RPA and hybrid functional calculations are in good agreement with the experimental results, and they explain the long-standing contradiction between the diffusion barriers derived from experiment and obtained in calculations with semilocal XC functionals. This shows that the semilocal functionals overestimate binding at the transition state more than they do at the energy minimum.

C. Au_N clusters ($N = 2$–6) supported on pristine and F_s-defected MgO(100) surface

A density functional/basin-hopping[31] (DF-BH) global optimization algorithm implemented in the FHI-aims code[69,89] was initially used to locate the lowest-energy structures (as well as high-energy isomers) of gas-phase Au_N clusters up to 6 atoms. The potential energy surface was calculated using the PBE functional. This procedure allowed us to corroborate planar geometries as global minima for clusters of this size.[90,91] The Au_N clusters with these geometries were placed on both pristine and neutral F_s-defected MgO(100) surfaces (using periodic models) and subjected to PBE relaxation. We considered two different groups of starting configurations: (a) *parallel* to oxide surface, where the Au_N cluster is positioned lying horizontal to the oxide, with all cluster Au atoms in contact with the surface; (b) in a *vertical* position, where the Au_N cluster is positioned perpendicular to the oxide surface.

In each group, structures with three or four different initial arrangements (depending on the Au_N cluster size) were considered for the periodic PBE relaxations. Moreover, the lowest-energy Au_5 and Au_6 supported clusters were further corroborated as global minima (GM) by another DF-BH scheme, which has been recently used to successfully locate the GM structures of small Au_N clusters supported on MgO(100).[31,92] The relaxed GM configurations of supported Au_N ($N = 2$–6) clusters found using the periodic approach (PBE) were then used with our MgO cluster models for single-point calculations using the EX-cRPA/cRPA+, hybrid (PBE0 and HSE06), and semilocal (PBE and RPBE) functionals.

D. Supported Au_N clusters structural motifs

In agreement with previous work,[11,12] the Au_N clusters preserve much of the planar character of the corresponding lowest-energy gas-phase structures upon adsorption at the pristine MgO(100) surface, binding perpendicular to the oxide surface (see Fig. 4). The vertical orientation of the adsorbed clusters is preferred due to increased polarizability in the direction perpendicular to the surface, optimizing interaction with the Madelung field (so-called "metal-on-top" stabilization mechanism[11,12]). Iterative Hirshfeld (Hirshfeld-I)[93] analysis of the PBE charge density reveals that the adsorbed clusters become slightly negatively charged, as a result of a small charge transfer from the oxide surface (see Fig. 5).[94,95] In fact, the charge transfer is so small that it is most probably a result of polarization rather than actual charge transfer. Small elongations on the Au-Au bond lengths are observed between Au atoms in direct contact with the surface, revealing that a strain occurs in order to maximize interaction with the surface anionic sites.

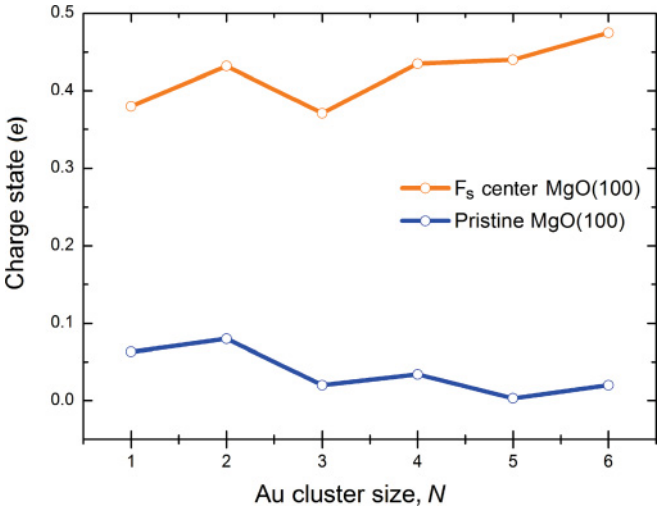

FIG. 5. (Color online) Electron excess (obtained by Hirshfeld-I analysis) on an Au adatom and Au_N clusters ($N = 2$–6), supported at both pristine (blue color line) and F_s-defected (orange color line) MgO(100) cluster surfaces. Charge is expressed in units of e, positive sign denotes excess of electrons (*negative* actual charge).

At the F_s center, the changes in the geometry of the supported clusters compared to the gas phase are more pronounced: the Au atoms that do not directly touch the surface are pulled closer to the vacancy (see Fig. 6). The electron transfer to the gold clusters adsorbed at the F_s center is also much more pronounced. Hirshfeld-I analysis of the PBE electron density reveals that between 0.35 and 0.5 the electron is transferred to the Au_N clusters depending on the size, with the largest transfer for the largest cluster size considered (see Fig. 5).

For each supported Au_N cluster, the following structural trends are observed:

Au_2. On the pristine surface, the lowest-energy configuration corresponds to an Au_2 dimer bound to one oxygen surface atom, perpendicular to the MgO(100) surface (Fig. 4). One Au atom is bound to an oxygen surface atom at a distance of 2.166 Å, while the dimer bond length remains practically unchanged (2.507 Å) compared to the gas-phase structure (2.511 Å), in good agreement with previous theoretical results.[11,49,52,96–98] The ground state of both gas-phase and supported Au_2 is a singlet. Furthermore, due to the strong attractive interaction at the F_s center, the most stable Au dimer configuration is tilted toward an Mg surface atom (67° to the surface normal), with an elongated dimer bond length of 2.70 Å, compared to the dimer supported on the pristine surface (see Fig. 6). Stable upright and tilted (33° to the surface normal) Au_2 dimers adsorbed on the oxygen vacancy have also been recently reported in literature.[11,97]

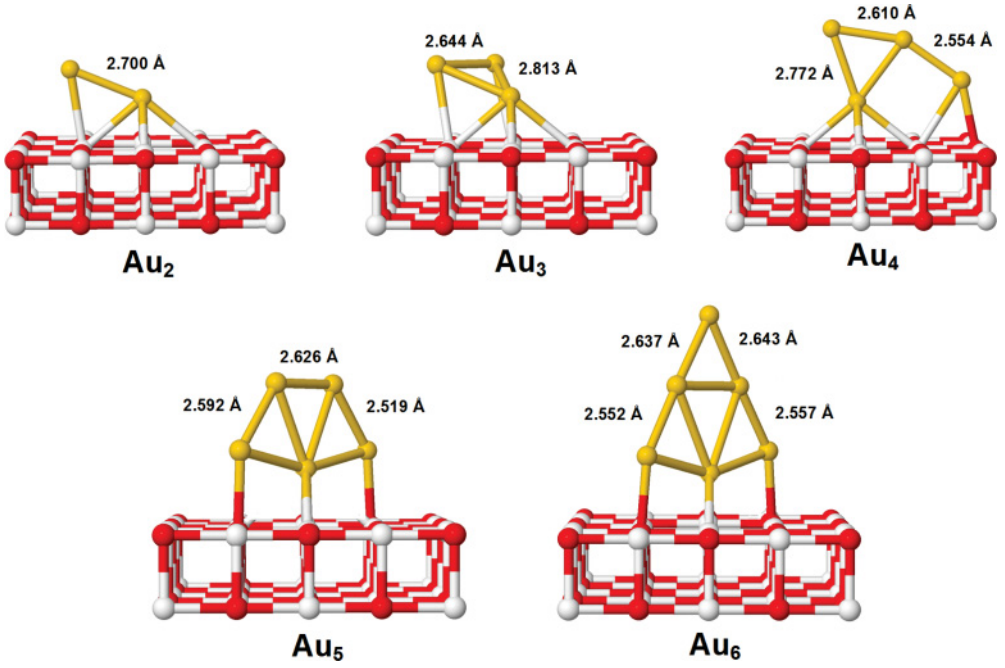

FIG. 6. (Color online) Lowest-energy structures (PBE) of Au_N ($N = 2$–6) clusters supported on a F_s-defected $Mg_{25}O_{24}$ cluster surface. Bond distances are expressed in Å.

Au$_3$. On the pristine surface, an acute triangular structure (angle of 81.29°) perpendicular to the oxide surface is found as the lowest-energy configuration. It binds to two oxygen surface atoms at a distance of 2.29 Å (see Fig. 4). A similar structure has been reported in previous computational studies.[11,50,52] At the F_s center, an equilateral triangle, largely tilted with respect to the MgO surface, is found as the lowest-energy configuration, in perfect agreement with previous theoretical work.[12,49,51,52] However, the calculated E_{adh} values tend to differ due to the XC choice and DFT approach, e.g., plane waves versus all-electron full-potential calculations.

Au$_4$. At the pristine surface, the lowest-energy configuration resembles an obtuse triangular structure, as found for Au_3, with one capped Au atom, as previously reported in literature.[50–52,98] This geometry is obtained when relaxation is started from both rhombohedral and three-dimensional (3D) tetrahedral geometries, which are both local minima in the gas phase, with the planar geometry being 1.34 eV more stable (at PBE level). The relaxed Au_4 cluster is bound to two surface oxygen atoms by direct interaction of the two Au atoms close to the surface (see Fig. 4). At the F_s center, the most stable configuration corresponds to a distorted rhombohedral structure, similar to the case of the pristine surface, but in this case one of the two lower Au atoms is bound to the vacancy, and the other one is bound to an anion surface site. Our results agree with previous computational studies, which found the same structure as global minimum,[12,52] with other rhombohedral-type motifs being higher in energy.[12,51]

Au$_5$. The most stable Au_5 cluster supported on the pristine oxide has a planar flipped "W"-shaped structure, bound to three oxygen surface atoms, perpendicular to the MgO(100) surface. It remains practically unchanged upon adsorption compared to its corresponding gas-phase structure (small, <0.1 Å, elongations of the Au-Au distances between the three Au atoms directly interacting with the surface). The preference for the oxide-supported Au pentamer to adopt this configuration is further confirmed by our DF-BH (PBE) global optimization searches, and is in agreement with recent theoretical work.[51,52] An Au_5 cluster strongly interacts with the F_s center, with distortions from the gas-phase structure being much more pronounced (see Fig. 6). Similar structures for the Au_5 cluster adsorbed at oxygen vacancy have been obtained using the PW91 and RPBE functionals (see Refs. 51 and 52).

Au$_6$. The lowest-energy configuration at the pristine surface is planar, perpendicular to the surface, with three Au atoms bound to three oxygen surface sites (see Fig. 4), in agreement with previous work,[52] but in contradiction with RPBE calculations in Ref. 51, where an inverted structure, with single Au atom in contact with the surface, was found more stable. When adsorbed on the F_s center, the Au_6 cluster is locally distorted, but globally has the same shape, similar to the Au_5 cluster. This is again in agreement with previous work.[12,52,92]

E. Supported Au_N clusters adhesion energies

**From Tables V and VI, and Figs. 7 and 8, it can be noted that adhesion energies calculated with hybrid functionals are systematically smaller than PBE values for Au clusters, similar to the single Au atom case. This is as expected since the reasoning used to explain this difference for the Au atom should be also applicable to larger Au clusters. However, while for the single atom the EX-cRPA/cRPA+ adhesion energies are *smaller* than PBE values, for the larger clusters

TABLE V. Calculated E_{adh} values for the most stable Au_N clusters supported on a pristine $Mg_{25}O_{25}$ cluster surface, calculated using various XC functionals.

E_{adh} (eV)	RPBE	PBE0	HSE06	PBE	EX-cRPA/ cRPA+	PBE–vdW
Au_2	0.99	1.22	1.24	1.35	1.38/1.34	1.47
Au_3	1.04	1.45	1.48	1.68	1.70/1.63	1.79
Au_4	1.44	1.95	1.97	2.13	2.25/2.17	2.30
Au_5	0.77	1.28	1.32	1.53	1.71/1.62	1.66
Au_6	0.72	1.31	1.34	1.50	1.78/1.69	1.65

EX-cRPA/cRPA+ gives *larger* adhesion energies compared to PBE, with the difference increasing with cluster size. This trend is especially clear for clusters adsorbed on the F_s-defected surface. Apparently, another type of interaction starts to play an important role for clusters of larger size. A candidate for this new contribution could be van der Waals interaction since it is present in EX-cRPA/cRPA+, but not in PBE or the hybrid functionals. To check this, we apply the recently developed Tkatchenko-Scheffler (TS–vdW) correction scheme.[68] In this scheme, vdW interactions are accounted for through the C_6R^{-6} terms, and C_6 coefficients and vdW radii of the interacting atoms are calculated from DFT ground-state electron density and reference values for free atoms. In our case, we apply the correction based on PBE electron density. Indeed, we find that the PBE–vdW E_{adh} values are close to those calculated using EX-cRPA/cRPA+, with differences from 0.09 to 0.16 eV for the pristine surface (Fig. 7), and 0.09–0.41 eV for the F_s-defected surface.

The larger differences are obtained for Au_5 and Au_6 clusters adsorbed on the vacancy, but they are still smaller than the differences between EX-cRPA/cRPA+ and PBE. The reason for these larger differences is that the electrons inside the vacancy are partitioned among all the atoms surrounding the vacancy, which may lead to underestimation of the vdW correction. Furthermore, energy differences between PBE–vdW and EX-cRPA/cRPA+ could be reconciled by the use of more accurate vdW coefficients, as recently calculated for ionic and semiconductor solids.[99] Thus, our results show that the vdW contribution to the interaction between gold clusters and the MgO surface increases with cluster size, and will eventually become dominant, in particular for the pristine surface.

TABLE VI. Calculated E_{adh} values for the most stable Au_N clusters supported on a F_s-defected $Mg_{25}O_{24}$ cluster surface, using various XC functionals.

E_{adh} (eV)	RPBE	PBE0	HSE06	PBE	EX-cRPA/ cRPA+	PBE–vdW
Au_2	2.46	2.84	2.85	2.99	3.30/3.21	3.21
Au_3	2.82	3.32	3.33	3.45	3.97/3.87	3.75
Au_4	3.65	4.19	4.21	4.30	4.79/4.68	4.62
Au_5	2.92	3.56	3.58	3.73	4.22/4.10	3.89
Au_6	2.61	3.35	3.35	3.46	4.07/3.94	3.66

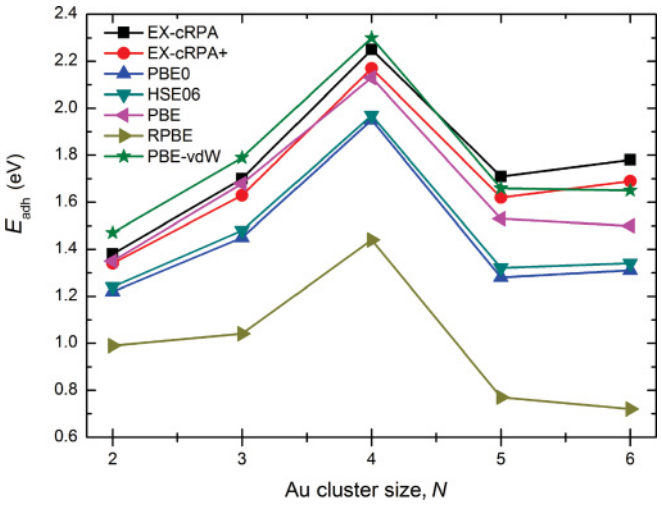

FIG. 7. (Color online) Calculated E_{adh} values for Au_N (N = 2–6) clusters supported on a pristine $Mg_{25}O_{25}$ cluster surface.

From the above discussion, it becomes clear that the seemingly worse performance of hybrid functionals for the adsorbed Au clusters compared to PBE is due to the artificial overestimation of the cluster-surface binding resulting from the self-interaction error in PBE. On the other hand, RPBE performs much worse than PBE or hybrid functionals, indicating that RPBE should be used with caution for this type of system.

One can also see from Figs. 7 and 8 that the adhesion energy increases with size for Au clusters containing up to four atoms, but then becomes smaller again for the larger clusters. One distinguishing feature of Au_5 and Au_6 is that there are two Au-Au bonds under strain to match the nearest-neighbor anion distance at the surface, while for the other clusters there is maximum one Au-Au bond under strain. Therefore, we believe it is the strain that reduces the adhesion of the larger clusters to the surface. This also implies that surface strain can affect the stability of adsorbed metal clusters.

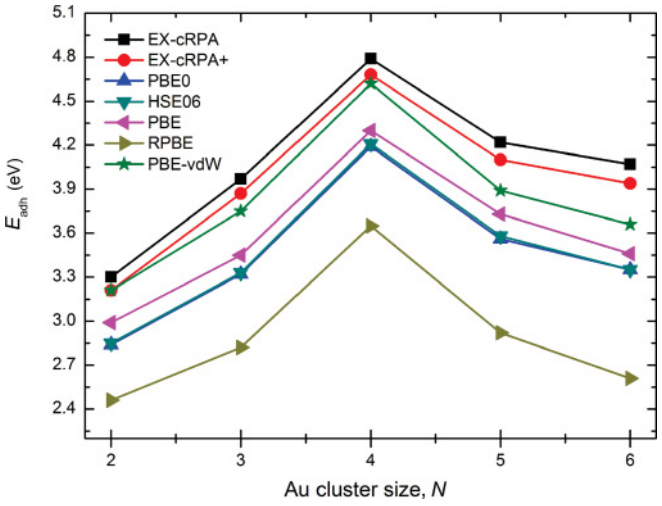

FIG. 8. (Color online) Calculated E_{adh} values of Au_N (N = 2–6) clusters supported on a F_s-defected $Mg_{25}O_{24}$ cluster surface.

IV. CONCLUSIONS

In this work, we go two steps above the current semilocal DFT-based calculations in determining the E_{adh} values of an Au adatom and Au_N clusters ($N = 2$–6) supported on pristine and F_s-defected MgO(100) surfaces. In particular, we apply the "beyond-DFT" approach EX-cRPA/cRPA+. At the same time, we do not use any pseudopotential, effective core potential, or frozen core approximations, but treat all electrons on equal footing. We also report a systematic study of the performance of hybrid functionals for this type of systems by applying PBE0 and HSE06 functionals. Furthermore, we use a dispersion-corrected DFT scheme (TS–vdW) to explain the significantly larger adhesion energies obtained by EX-cRPA/cRPA+ for larger clusters, in terms of vdW interactions.

From our study we conclude the following:

(1) Reduction of SIE due to inclusion of exact exchange in hybrid functionals and EX-cRPA/cRPA+ results in smaller calculated adhesion energy for an Au adatom on both pristine and F_s-defected MgO(100) terraces, when compared to PBE. This effect is larger for the Au adatom at the transition state along the minimum energy path between two local adsorption basins, resulting in an increase of the calculated barrier for the Au adatom diffusion along the surface. Although the increase in the diffusion barrier is small (0.06 eV compared to PBE), it reconciles the experimental onset temperature for Au cluster formation[55] with theoretical predictions based on temperature-induced hopping model. It also explains the discrepancy between the onset temperature derived from diffusion barriers calculated using semilocal functionals and the experimental onset temperature.

(2) The lowest-energy structures of small Au_N clusters ($N = 2$–6), supported on both the pristine and neutral F_s-defected MgO(100), align vertical to the MgO(100) surface due to a metal-on-top effect.[11,12] They preserve much of the planar character of their corresponding gas-phase structures, with larger structural distortions when adsorbed at the F_s center. Calculated E_{adh} for adhesion at neutral F_s centers is found to be larger by 1.9–2.5 eV at the EX-cRPA+ level, depending on cluster size. The adhesion energy decreases for cluster sizes larger than four because the larger clusters must be strained to be accommodated at the surface.

(3) Contrary to the single Au atom case, the calculated EX-cRPA/cRPA+ E_{adh} values for Au_N clusters, supported at both pristine and F_s-defected surfaces, are larger than those calculated using the semilocal PBE and hybrid (PBE0 and HSE06) XC functionals. This is rationalized in terms of increasing importance of vdW contributions to the E_{adh} values (accounted for in EX-cRPA/cRPA+) and the progressively smaller influence of SIE for Au_N clusters larger than the single atom.[100,101]

Finally, we note that a structural transition from 2D to 3D oxide-supported Au_N clusters, at sizes larger than those here considered, is expected due to the strong interaction between the F_s center and the small Au_N clusters, causing the vertical and horizontal planar Au_N structures to distort from planarity, as observed by Yoon *et al.*[41] A more extensive study is needed to elucidate the exact size at which this transition occurs.

ACKNOWLEDGMENTS

This work has been funded by the DFG through the Cluster of Excellence Unifying concepts in Catalysis (UniCat). Calculations were performed at the Rechenzentrum Garching (RZG) of the Max Planck Society and the IPP, using the IBM pSeries Power6 high-performance computer. The authors acknowledge M. Scheffler and A. Tkatchenko (FHI, Berlin) for valuable feedback on a draft of this article and X. Ren for technical assistance regarding the RPA/RPA+ calculations. H. Freund (FHI, Berlin) is also acknowledged for relevant discussions when comparing our DFT versus experimental results.

*borbon@fhi-berlin.mpg.de

[1] M. Haruta, T. Kobayashi, H. Sano, and N. Yamada, Chem. Lett. **16**, 405 (1987).
[2] G. Bond, C. Louis, and D. Thompson, *Catalysis by Gold* (Imperial College Press, London, 2006).
[3] G. Bond, Gold Bull. **5**, 11 (1972).
[4] T. Hayashi, K. Tanaka, and M. Haruta, J. Catal. **178**, 566 (1998).
[5] M. Valden, X. Lai, and D. Goodman, Science **281**, 1647 (1998).
[6] T. Salama, R. Ohnishi, T. Shido, and M. Ichikawa, J. Catal. **162**, 169 (1996).
[7] D. Andreeva, V. Idakeiv, T. Tabakova, A. Andreev, and R. Giovanolli, Appl. Catal., A **134**, 275 (1996).
[8] H. Falsig, H. Hvolboek, I. Kristensen, T. Jiang, T. Bligaard, C. Christensen, and J. Nørskov, Angew. Chem. **120**, 4913 (2008).
[9] G. Bond and D. Thompson, Gold Bull. **33**, 41 (2000).
[10] M. Haruta, CATTECH **6**, 102 (2002).
[11] G. Barcaro and A. Fortunelli, J. Chem. Theory Comput. **1**, 972 (2005).
[12] G. Barcaro and A. Fortunelli, J. Phys. Chem. B **110**, 21021 (2006).
[13] M. Chen and D. Goodman, Acc. Chem. Res. **39**, 739 (2006).
[14] H.-J. Freund, Surf. Sci. **500**, 271 (2002).
[15] R. Meyer, C. Lemire, S. K. Shaikhutdinov, and H.-J. Freund, Gold Bull. **37**, 72 (2004).
[16] C. Henry, Surf. Sci. Rep. **31**, 231 (1998).
[17] J. Libuda and H.-J. Freund, Surf. Sci. Rep. **57**, 157 (2005).
[18] C. Barth and C. R. Henry, Phys. Rev. Lett. **91**, 196102 (2003).
[19] G. Pacchioni, Chem. Phys. Chem. **4**, 1041 (2003).
[20] T. Risse, S. K. Shaikhutdinov, N. Nilius, M. Sterrer, and H.-J. Freund, Acc. Chem. Res. **41**, 949 (2008).
[21] A. Kolmakov, J. Stultz, and D. Goodman, J. Phys. Chem. **113**, 7564 (2000).
[22] U. Martinez, L. Giordanio, and G. Pacchioni, J. Phys. Chem. B **110**, 17015 (2006).
[23] Z. Yan, S. Chinta, A. Mohamed, J. Fackler, and D. Goodman, J. Am. Chem. Soc. **127**, 1604 (2005).
[24] M. Mavrikakis, P. Stolze, and J. Nørskov, J. Catal. Lett. **64**, 101 (2005).
[25] J. Nørskov, T. Bligaard, B. Hvolbak, F. Abild-Pedersen, I. Chorkendorff, and C. Christensen, Chem. Soc. Rev. **37**, 2163 (2008).

[26]M. Frank, M. Baumer, R. Kuehnemuth, and H.-J. Freund, J. Phys. Chem. B **105**, 8569 (2001).
[27]A. Ferrari and G. Pacchioni, J. Phys. Chem. **92**, 096105 (1996).
[28]H.-J. Freund and G. Pacchioni, Chem. Soc. Rev. **37**, 2224 (2008).
[29]M. Moseler, H. Häkkinen, and U. Landman, Phys. Rev. Lett. **89**, 176103 (2002).
[30]B. Huber, P. Koskinen, H. Häkkinen, and M. Moseler, Nat. Mater. **5**, 44 (2006).
[31]G. Barcaro, E. Aprà, and A. Fortunelli, Chem. Eur. J. **13**, 6408 (2007).
[32]L. Giordano and G. Pacchioni, Surf. Sci. **575**, 197 (2005).
[33]G. Barcaro and A. Fortunelli, Phys. Rev. B **76**, 165412 (2007).
[34]H.-J. Freund, H. Kuhlenbeck, J. Libuda, G. Rupprechter, M. Baaumer, and H. Hamann, Top. Catal. **15**, 201 (2001).
[35]D. Starr, S. K. Shaikhutdinov, and H.-J. Freund, Top. Catal. **36**, 33 (2005).
[36]G. Barcaro and A. Fortunelli, J. Phys. Chem. C **111**, 11384 (2007).
[37]G. Barcaro, M. Causà, and A. Fortunelli, Theor. Chem. Acc. **118**, 807 (2007).
[38]C. Harding, V. Habibpour, S. Kunz, A.-S. Farnbacher, U. Heiz, B. Yoon, and U. Landman, J. Am. Chem. Soc. **131**, 538 (2009).
[39]A. Sanchez, S. Abbet, U. Heiz, W.-D. Schneider, H. Häkkinen, R. Barnett, and U. Landman, J. Phys. Chem. A **103**, 9573 (1999).
[40]B. Yoon, H. Häkkinen, and U. Landman, J. Phys. Chem. A **107**, 4066 (2003).
[41]B. Yoon, H. Häkkinen, U. Landman, A. Warz, J. Antonietti, S. Abbet, K. Judai, and U. Heiz, Science **307**, 403 (2005).
[42]I. Remediakis, N. Lopez, and J. Nørskov, Appl. Catal., A **291**, 13 (2005).
[43]B. Hammer and J. Nørskov, Nature (London) **376**, 238 (1995).
[44]L. M. Molina and B. Hammer, Phys. Rev. B **69**, 155424 (2004).
[45]H. Häkkinen, S. Abbet, A. Sanchez, U. Heiz, and U. Landman, Angew. Chem., Int. Ed. **42**, 1297 (2003).
[46]N. Lopez and J. Nørskov, J. Am. Chem. Soc. **124**, 11262 (2002).
[47]N. Lopez, T. Janssens, B. Clausen, Y. Xu, M. Mavrikakis, T. Bligaard, and J. Nørskov, J. Catal. **223**, 232 (2004).
[48]I. Yudanov, G. Pacchioni, K. Neyman, and N. Rösch, J. Phys. Chem. B **101**, 2786 (1997).
[49]A. Del Vitto, G. Pacchioni, F. Delbecq, and P. Sautet, J. Phys. Chem. B **109**, 8040 (2005).
[50]G. Barcaro and A. Fortunelli, New J. Phys. **9**, 22 (2007).
[51]P. Frondelius, H. Häkkinen, and K. Honkala, New J. Phys. **9**, 339 (2007).
[52]L. Molina and J. Alonso, J. Phys. Chem. C **111**, 6668 (2007).
[53]A. Fortunelli and R. Ferrando, *in Nanoparticles*, edited by R. L. Johnston and J. Wilcoxon (Elsevier, Amsterdam, 2012).
[54]M. Yulikov, M. Sterrer, M. Heyde, H.-P. Rust, T. Risse, H.-J. Freund, G. Pacchioni, and A. Scagnelli, Phys. Rev. Lett. **96**, 146804 (2006).
[55]M. Yulikov, M. Sterrer, T. Risse, and H.-J. Freund, Surf. Sci. **603**, 1622 (2009).
[56]J. P. Perdew and A. Zunger, Phys. Rev. B **23**, 5048 (1981).
[57]A. Cohen, P. Mori-Sanchez, and W. Yang, J. Chem. Phys. **126**, 191109 (2007).
[58]J. Harl, L. Schimka, and G. Kresse, Phys. Rev. B **81**, 115126 (2010).
[59]J. Harl and G. Kresse, Phys. Rev. Lett. **103**, 056401 (2009).
[60]X. Ren, P. Rinke, and M. Scheffler, Phys. Rev. B **80**, 045402 (2009).
[61]M. Rohlfing and T. Bredow, Phys. Rev. Lett. **101**, 266106 (2008).
[62]F. Furche, Phys. Rev. B **64**, 195120 (2001).
[63]M. Fuchs and X. Gonze, Phys. Rev. B **65**, 235109 (2002).
[64]P. Garcia-Gonzalez, J. Fernandez, A. Marini, and A. Rubio, J. Phys. Chem. A **111**, 12458 (2007).
[65]J. F. Dobson, A. White, and A. Rubio, Phys. Rev. Lett. **96**, 073201 (2006).
[66]L. Schimka, J. Harl, A. Stroppa, A. Gruneis, M. Marsman, F. Mittendorfer, and G. Kresse, Nat. Mater. **9**, 741 (2010).
[67]S. Kurth and J. P. Perdew, Phys. Rev. B **59**, 10461 (1999).
[68]A. Tkatchenko and M. Scheffler, Phys. Rev. Lett. **102**, 073005 (2009).
[69]V. Blum, R. Gehrke, F. Hanke, P. Havu, V. Havu, X. Ren, K. Reuter, and M. Scheffler, Comput. Phys. Commun. **180**, 2175 (2009).
[70]E. V. Lenthe, E. Baerends, and J. Snijders, J. Chem. Phys. **101**, 9783 (1994).
[71]J. Perdew, A. Ruzsinszky, J. Tao, V. Staroverov, G. Scuseria, and G. Csonka, J. Chem. Phys. **123**, 062201 (2005).
[72]J. P. Perdew, K. Burke, and M. Ernzerhof, Phys. Rev. Lett. **77**, 3865 (1996).
[73]B. Hammer, L. B. Hansen, and J. K. Nørskov, Phys. Rev. B **59**, 7413 (1999).
[74]J. Perdew, K. Burke, and M. Ernzerhof, J. Chem. Phys. **105**, 9982 (1996).
[75]C. Adamo and V. Barone, J. Chem. Phys. **110**, 6158 (1999).
[76]T. Henderson, A. Izmaylov, G. Scalmani, and G. Scuseria, J. Chem. Phys. **131**, 044108 (2009).
[77] In FHI-aims, the Kohn-Sham orbitals are expanded in basis sets consisting of numerical atom-centered orbitals (NAO's). These correspond to preconstructed hierarchical basis sets (*minimal, tier* 1, . . . , *tier* 3). They list a number of radial functions (and their) angular momenta, e.g., *tier* 1 consist of a minimal basis set plus one additional valence *s, p*, and *d* functions (also called "double numeric plus polarization"). In this way, *tier* 2 includes another set of *s,p,d* functions as well as *f* and *g*, thus improving convergence with respect to basis set up to meV for calculated energy differences. Furthermore, *light* and *tight* settings refer to specific parameters regarding the *confinement radius* of the radial functions, the multipole expansion of the *Hartree potential*, and the number of grid points used in the *integration grid*.
[78]N. Lopez, F. Illas, N. Rosch, and G. Pacchioni, J. Chem. Phys. **110**, 4873 (1999).
[79]S. Boys and F. Bernardi, Mol. Phys. **19**, 553 (1970).
[80]H. Grönbeck and P. Broqvist, J. Phys. Chem. B **107**, 12239 (2003).
[81]M. Sterrer, E. Fischbach, T. Risse, and H.-J. Freund, Phys. Rev. Lett. **94**, 186101 (2005).
[82]N. Nilius, Surf. Sci. Rep. **64**, 595 (2009).
[83]A. Becke, J. Chem. Phys. **98**, 5648 (1993).
[84]C. Di Valentin, A. Scagnelli, G. Pacchioni, T. Risse, and H.-J. Freund, Surf. Sci. **600**, 2434 (2006).
[85]R. Ferullo, S. Fuente, P. Belelli, and N. Castellani, Surf. Sci. **603**, 1262 (2009).
[86]H. Benia, X. Lin, H.-J. Gao, N. Nilius, and H.-J. Freund, J. Phys. Chem. C **111**, 10528 (2007).
[87]L. Romaner, X. Ren, C. Ambrosch-Draxl, and M. Scheffler (unpublished).
[88]V. Musolino, A. Selloni, and R. Car, J. Chem. Phys. **108**, 5044 (1998).
[89]R. Gehrke and K. Reuter, Phys. Rev. B **79**, 085412 (2009).
[90]H. Häkkinen, B. Yoon, U. Landman, X. Li, H. Zhai, and L. Wang, J. Phys. Chem. A **107**, 6168 (2003).

[91]E. M. Fernández, J. M. Soler, I. L. Garzón, and L. C. Balbás, Phys. Rev. B **70**, 165403 (2004).
[92]G. Barcaro and A. Fortunelli, Chem. Phys. Lett. **457**, 143 (2008).
[93]P. Bultinck, P. Ayers, S. Fias, K. Tiels, and C. V. Alsenoy, Chem. Phys. Lett. **444**, 205 (2007).
[94]F. Hirshfeld, Theor. Chim. Acta **44**, 129 (1977).
[95]P. Bultinck, C. V. Alsenoy, P. Ayers, and R. Carbó-Dorca, J. Chem. Phys. **126**, 144111 (2007).
[96]R. Caballero, C. Quintanar, A. Koster, S. Khanna, and U. Reveles, J. Phys. Chem. C **112**, 14919 (2008).
[97]M. Walter and H. Häkkinen, Phys. Rev. B **72**, 205440 (2005).
[98]P. Frondelius, H. Häkkinen, and K. Honkala, Phys. Rev. B **76**, 073406 (2007).
[99]G. X. Zhang, A. Tkatchenko, J. Paier, H. Appel, and M. Scheffler, Phys. Rev. Lett. **107**, 245501 (2011).
[100]R. Ferrando, G. Barcaro, and A. Fortunelli, Phys. Rev. Lett. **102**, 216102 (2009).
[101]R. Ferrando, G. Barcaro, and A. Fortunelli, Phys. Rev. B **83**, 045418 (2011).